Research Article

SOHAG JOURNAL OF SCIENCES

https://doi.org/10.21608/sjsci.2024.243738.1138

Highly Selective Conversion of Isopropanol to Propene Over $CeFeO_3$/Spherical Silica Nanocomposite

Walaa A. ElHamdy[1,*], Abd El-Aziz A. Said[2] and Kamal M. S. Khalil[1]

[1] *Chemistry Department, Faculty of Science, Sohag University, Sohag 82524, Egypt*
[2] *Chemistry Department, Faculty of Science, Assiut University, Assiut 71516, Egypt*
**Email: walaaelhamdy@yahoo.com*

Received: 26th October 2023 **Revised:** 20th Nivember 2023 **Accepted:** 1st January 2024
Published online: 30th January 2024

Abstract: Cerium iron mixed oxide (CFO) nanocomposite materials supported on spherical silica particles were explored for gas phase dehydration of isopropyl alcohol (IPA). The samples were formed by a sol-gel process. Utilization of silica as a matrix for reducible CeO_2-Fe_2O_3 mixed oxides formation of thermally stabilized textural CeO_2-Fe_2O_3 /silica nanocomposite materials, Thus, a series of 10-30% (w/w) CFO/silica was directly formed, dried, and calcined at 550ºC. XRD, TG-DTA, ATR-FTIR, nitrogen adsorption−desorption, and TEM images were used to analyze the samples. The catalytic performance of materials has been estimated. The catalytic activity of the catalytic materials was evaluated to measure the dehydration reaction of IPA at 250 ºC in the air atmosphere. According to the results, 20% $CeFeO_3$/silica calcined at 550ºC exhibits a high conversion of IPA amounts to ~89% with selectivity (100%) for propene, as well as a high rate of propene production (7.9 m mol.h^{-1}). The higher catalytic activity of the supported catalyst was related to its improved textural and thermal stability, based on these results, propene is efficiently produced.
Keywords: mixed oxide, spherical silica, nanocomposite, IPA, propene.

1. Introduction

The a high demand for lower olefins, which are fundamental elements of the chemical industry and have a wide range of industrial uses (including synthetic fibers, anti-freezing agents, packaging materials, and solvents) **[1]**. Thus, the process of converting short-chain alcohols (such as methanol, ethanol, butanol, isopropanol, etc.) to olefin is one of the ideal approaches for developing novel, environmentally friendly technologies for generating lower olefins to supplement the limited petroleum feedstock supply**[2, 3]**.

The need for polypropylene up to 64% and their derivatives from propylene oxide, acrylonitrile, oxo alcohol, and others reach 36% increases annually **[4]**, raising the global production rate of propylene by 4–5%. In the chemical industry, propene is regarded as one of the fundamental ingredients because it is used to make many significant products, including polypropene and propene oxide **[5]**. Steam thermal cracking of naphtha, catalytic cracking of C4 alkenes **[6]**, catalytic propene dehydrogenation **[7],** and catalytic dehydration of IPA **[8, 9]** are the processes used in the industrial manufacture of propene. For catalytic dehydration of IPA to propene, solid acid catalysts for instanceWO_3/ZrO_2**[10]**, Al_2O_3-TiO_2 **[11]**, WO_3/ACP **[12]**, phosphate zeolite **[13]** and $Fe_2O_3/\gamma Al_2O_3$[14] have been employed as catalyst. Significant thermal mechanical chemical properties, the surface characteristics, and morphology of SiO_2 materials **[15]** succeed in the utilization of silica as catalyst support Therefore, Numerous heterogeneous catalysis methods have recently been investigated as prospective support catalysts for petrochemical, as well as petrochemical processes **[16–18]** and gas-liquid-phase oxidation processes **[19]**. However, it has some drawbacks due to hydrothermal activity reactivity **[20]**. Additionally, the supporting phenomena can be advantageous when loading an active phase on support **[21–23]**. Thus, active phases have become the research focus.

It has been found that doping silica with cerium has a positive impact on enhancing ment redox properties of ceria **[24]**. The catalytic activity of ceria-based materials due to their redox behavior (Ce^{4+}/Ce^{3+}) and the ability of formation of oxygen vacancies for improving structural and chemical properties doping ceria with iron due to its redox behavior **[25]**. Numerous reports that cerium iron mixed oxide composites have various uses in catalysis such as catalytic oxidation and photocatalytic degradation of nitroaromatic compounds **[26]**, which are highly affected by the preparation methods, iron content, sintering temperature, and phase composition **[27]**.

Some advanced applications have been explored for Cerium iron mixed oxide nanostructured, including photodegradation of Congo dye **[28]**, Selective catalytic reduction of NOx **[29]**, ozonation of nitrobenzene in water **[30]**, oxygen carrier and hydrogen generation[31,32] and photocatalyst **[33, 34]**. Several investigations have demonstrated that improving catalytic performance is significantly connected with the dispersion and particle size of the metal **[23, 35–37]**. Mixed oxides or perovskite have been utilized for modification of silica towards gas phase alcohol dehydration reaction. Perovskite oxide types are considered very promising catalytic materials owing to low cost, excellent

thermal stability, adjustable redox ability, and oxygen mobility. Lanthanum-iron mixed oxide perovskite has gained great interest in numerous catalytic applications including electro-catalysis catalytic oxidation [38, 39] and combustion of volatile organic compounds (VOCs) via catalysis [40].

The present study used direct dispersion of 10, 20, and 30% (w/w) Cerium-iron mixed oxides precursors into freshly formed Stöber silica particles. Utilization of silica as a matrix for reducible CeO_2-Fe_2O_3 mixed oxides formation of thermally stabilized textural CeO_2-Fe_2O_3 /silica nanocomposite materials that were calcined for three hours at 550°C using static air. many standard bulk and surface characterization methods were used to describe the supported catalysts. Examinations of the novel catalysts for isopropyl alcohol to propene gas phase dehydration. The surface structure and texture of supported catalysts correlate to their catalytic activity.

2. Materials and methods

Iron(III) nitrate nonahydrate, $Fe(NO_3)_3.9H_2O$, (assayed), 98%, solid product of (Prolabo, France); Cerium(III) nitrate hexahydrate, $Ce(NO_3)_3.6H_2O$; Citric acid, $C_6H_8O_7$ purified (Merck, India); tetraethyl orthosilicate, $Si(OC_2H_5)_4$, (TEOS), 98%, liquid,(Sigma-AldrichCompany, Ltd.,(Germany); isopropyl alcohol (IPA), pyridine (PY), 2,6-dimethyl pyridine (DMPY); Ethyl alcohol C_2H_5OH, 99.5%, (Adwic, Egypt) and 33% NH_3 aqueous ammonia solution (BDH, Ltd., England) were acquired and used exactly as directed.

2.1. Silica support synthesis

The Stöber method [41] was used to synthesize the blank silica material. The preparation process is described in further detail elsewhere [41–43]. Briefly, TEOS (19.0 mL) was dispersed into a solution containing absolute alcohol (207 mL) and ammonia (155 mL) after that, keep stirring continuously for 1 h with magnetic stirring (400 rpm), to produce freshly Stöber silica sol. The solution was filtered after being aged at ambient temperature for a week before being dried for a full day at 120 °C. The dry material was calcined for three hours in static air at a ramp rate of 1°C min^{-1} up to 550°C and labeled as silica support 550.

2.2. Synthesis of CFO/SiO_2 composite material

CFO/SiO_2 composite materials with weight percentages of 10, 20, and 30% were prepared as follows. computed amount of Fe $(NO_3)_3.9H_2O$,$Ce(NO_3)_3.6H_2O$, and $C_6H_8O_6$. H_2O was dissolved in 50 mL of water. The final product was mixed with recently produced silica sol. For one hour, the solution was swirled magnetically at 400 rpm. The finished mixture was allowed to sit at room temperature for a week. The resulting material was then filtered and dried at 120°C during the following day. Portions of dried material were maintained at this temperature of 550°C for three hours in the muffle furnace using static air at a ramp rate of 1°C min^{-1}. The calcined materials produced were referred to as calcined 10, 20, and 30% w% CFO/SiO2 550 composites.

2.3. Characterization Methodologies.

X-ray diffraction patterns were acquired using a diffractometer (a Phillips type Spectrometer version PW 2103/00 outfitted with a Ni-filtered, CuK radiation (=1.5418)) to confirm the structure and crystallinity of the materials, FTIR spectra have been detected utilizing. A 400-4000 cm-1 Bruker-Alpha FT-IR spectrometer (Germany).

Thermogravimetric analysis was performed on a TA 60 thermal analyzer apparatus (Shimadzu, Japan) at a heating rate of 10 °Cmin^{-1} and a flow rate of 30 mLmin^{-1} of air and nitrogen. At 196°C, nitrogen adsorption–desorption analyses were performed using a Micromeritics instrument (model ASAP 2010, Micromeritics Corporation, USA) Before measuring, test samples were degassed for 2 hours at 200 °C to 0.1Pa. The Brunauer-Emmett-Teller (BET) equation was used to get the specific surface area, SBET, was calculated by applying the Brunauer-Emmett-Teller (BET) equation[44]. The Barrett-Joyner-Halenda (BJH) method [45] was used to create the mesopore width distribution, and all measurements and analyses were carried out following IUPAC standards[46]. Transmission electron microscopy (TEM) image was tested using a 100kV Joel 2000 device. For EDX analysis, Oxford instrument X-MAX,80mm2.

2.4 Catalytic Performance Examination

The current composite catalysts' catalytic performance was examined for the Vapor phase dehydration of isopropanol employing chromatographic analysis by FID with a Unicam Pro GC2000 [12, 22, 47]. In a typical experiment 300 mg using of catalyst, in the temperature range120-250° C, air atmosphere as a carrier gas, and the total flow rate was 50 ml min^{-1}, 2.7 % isopropanol (IPA) in the gas feed and space-time (GHSV 10,000$mlg^{-1}h^{-1}$).

For calculation, the following formulas were used:

$$\text{IPA conversion (\%)} = \frac{[IPA]_{in}-[IPA]_{out}}{[IPA]_{in}} \times 100$$

$$\text{Propene Selectivity (\%)} = \frac{[\text{Propene}]}{[\text{propene}]+[\text{other products}]} \times 100$$

$$\text{Propene Yield (\%)} = \frac{\text{conversion} \times \text{Selectivity}}{100}$$

3. Results and Discussion:

3.1. XRD Diffractometer:

XRD diffraction patterns for blank silica support and the 10-30 CFO/silica composite's composites calcined at 550 °C for 3 h are displayed in Fig.1 The XRD patterns displayed blank silica support without additional peaks at the position characteristics for $CeFeO_3$ or CeO_2or Fe_2O_3 were observed. Furthermore, the broad peak at 25 attributes for silica was dramatically reduced as the CFO loading percentage was raised. The above observation for the supported catalysts suggests that CFO or mixed oxides were substantially scattered or present as extremely small nanoparticles of CFO, which were either amorphous or extremely small in comparison to the XRD detection limits [18].

3.1.2. FTIR spectra

FTIR spectra for 10, 20, and 30 CFO/Silica composite catalysts, along with silica support are shown in **Fig 2**. The spectrum displays several bands that exactly correlate to the silica gel band positions [43, 42]. The band at 3212 cm^{-1} corresponds to the ν(O–H) mode of (H–bonded) water

molecules. the band located at at1598 refers to the δ(OH) mode; the band at 940 cm^{-1} corresponds to ν(Si–OH); the bands at 1070 and 806cm^{-1} correspond to ν_{as} (Si–O–Si) and ν_s (Si–O–Si) modes, respectively; and the band at 446 cm^{-1} corresponds to the δ(Si–O–Si) mode. The band observed at 1430 cm^{-1} may be related to the presence of adsorbed nitrate species. However, As the CFO ratio increased, the intensity of the Si-OH *v* (962 cm^{-1}) band decreased slightly. This reduction in Si-OH vibration intensity suggests ongoing surface alteration of the silica substrate.

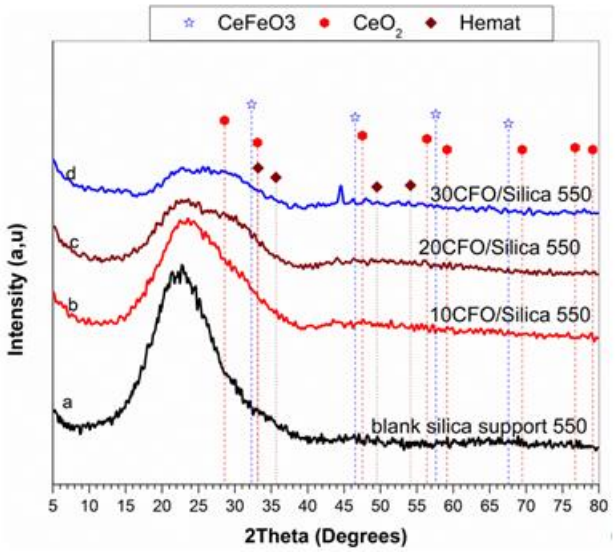

Fig. 1: XRD patterns of (a) Silica Support, (b) 10CFO/Silica, (c) 20CFO/Silica and (d) 30CFO/Silica 550.

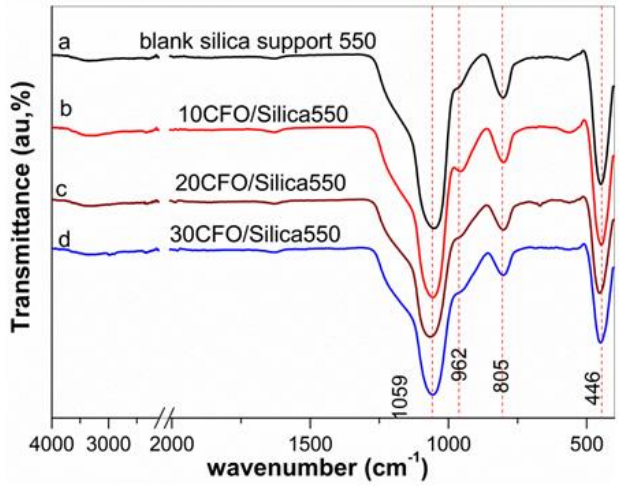

Fig. 2: FTIR-spectra for (a) Silica support, (b) 10CFO/Silica, (c) 20CFO/Silica, and (d) 30CFO/Silica 550.

3.1.3 Thermal Analysis (TGA and DTA)

Thermogravimetric and derivative thermogravimetric analyses (TGA and DTG) for 10, 20 and 30CFO/Silica composite materials with the corresponding silica support in N_2 and O_2 atmosphere, respectively are shown in **Fig. 3** (A and B), numerical data were listed in **Table S.1**. TGA curves reveal stable mass in the (200-750°C) range for SiO_2 support, whereas mass loss continues in this range for composite materials.

TGA–DTG results for 10, 20, and 30CFO/SiO_2 demonstrate three decomposition stages in each curve. Loss of adsorbed water is a result of the first stage below 150 °C. The range of the second stage of (170–400°C) was characterized by peaks at 227, 230, and 231 °C for 10, 20, and 30 CFO/SiO_2 in the N_2 atmosphere. However, in the O_2 atmosphere peaks were observed almost at the same position observed in N_2 typically at 225, 228, and 232 °C for 10, 20, and 30 CFO/SiO_2, respectively. The above results demonstrate that weight losses recorded in the N_2 atmosphere were more than those recorded in the O_2 atmosphere and DTG curves showed a peak around 230 for the composite materials in N_2 or air atmosphere, whereas such a peak was not observed at all for silica support. Data demonstrates that the thermal event at ~230 corresponded to the decomposition of the CFO precursor material and there was little effect of oxygen on that event.

Fig .4(A and B) show simultaneous DTA results for the above materials 10, 20, and 30CFO/SiO_2 in N_2 and O_2 atmosphere. In the flow of N_2, an exothermic peak was observed for the composite materials (but not for the blank silica) around 240 °C, Moreover, a shoulder peak was also observed around 300 °C. Similar exothermic peaks were observed in the flow of air at the same position 240C; however, no shoulders were accompanied by this peak. This suggests that the shoulders observed in the flow of N_2 were properly related to the composition of a minor number of organics (no weight loss was observed for this event).

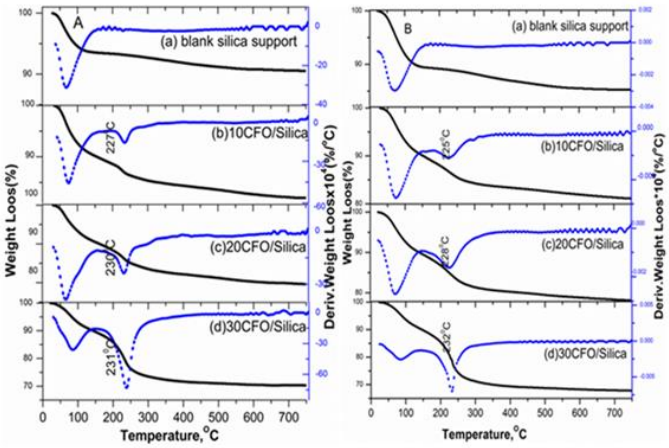

Fig. 3: TGA and DTG curves for uncalcined (a) Silica support,(b) 10CFO/Silica, (c)20CFO/Silica, and (d)30CFO/Silica in N_2 and O_2 atmosphere**.**

3.1.4 Nitrogen adsorption/desorption

The materials' textural properties were evaluated using N_2 adsorption-desorption isotherms in **Fig. 5** and **Table 1**. Silica support showed an Isotherm of type *II* with no discernible hysteresis loop based on the original IUPAC classification **[46]**. However, the composite catalytic materials showed isotherms of type *IV* isotherms with H_2 hysteresis loops. The surface area amounts to 25.6, 52.0, and 81.4 m_2g^{-1} were obtained for the 10, 20, and 30 CFO/silica catalyst, whereas a

small surface area amounts to 11.6 m2g-1 was obtained for the blank silica supports. Total pore volume V_p values (0.027,0.052 and 0.094) and external surface area S_t values (21.8,41.8 and 71.5) were obtained for the blank silica,10CFO/silica, 20CFO/silica and30CFO/silica, respectively. Total pore volume and external surface values follow the same order observed for S_{BET} surface area. Further textural characteristics including pore width distribution are shown in **Table 1**.

Pore width, and W_p, (via the average $4V_p/S_{BET}$ method and BJH method) were estimated, for the 10, 20, and 30 CFO/silica composite along with the silica support are depicted in Fig. 6. Values amounts to 108, 64, 62, and 54 were obtained by BJH method for the blank silica support, 10, 20 and 30 CFO/silica composite catalysts, respectively. Pore width distributions in the mesoporous range are presented in Fig.6.This observed trend demonstrates that the PWD was maximized in the higher and higher range of mesoporosity with increasing the loading ratio.

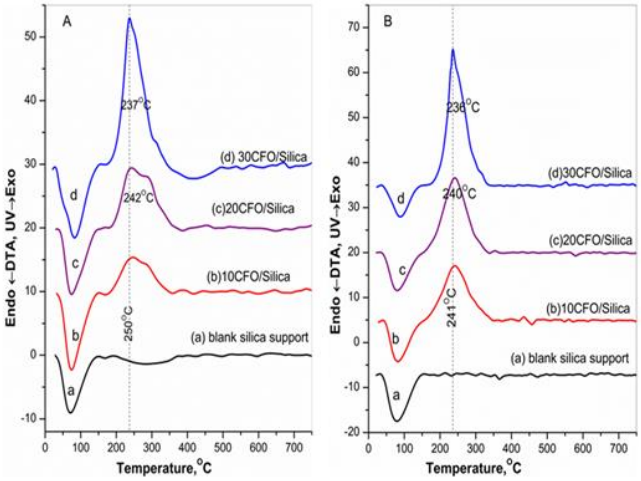

Fig. 4: DTA curves for uncalcined (a) Silica support,(b) 10CFO/Silica, (c)20CFO/Silica, and (d)30CFO/Silica in N_2 and O_2 atmosphere.

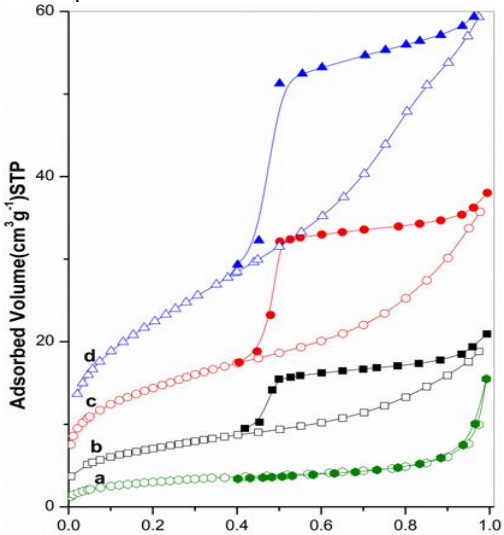

Fig. 5: N_2adsorption–desorption isotherms for calcined(a)Silica support, (b) 10CFO/Silica, (c) 20CFO/Silica and(d) 30 CFO /Silica550.

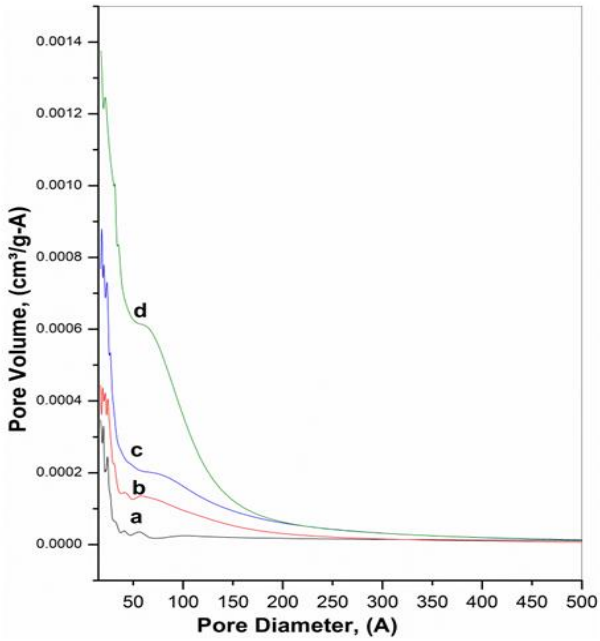

Fig. 6: Pore width dispersion for calcined (a) blank Silica,(b)10CFO/Silica, (c) 20CFO/Silica and (d) 30 CFO /Silica 550.

Table. 1: Textural characteristics for silica support and composites 550.

Samples	S_{BET} / m^2g^{-1}	C BET	V_p/cm^3g^{-1}	t-method m^2g^{-1}		Pore width W_p/ Å	
				S_{mic}	S_t	**4V/ S_{BET}**	BJH
Silica support 550	11.6	67.44	0.0118	0.166	10.99	42.2	108
10CFO/S550	25.6	107.3	0.027	3.7	21.8	42.4	64.1
20CFO/S550	52.00	126.70	0.052	10.2	41.8	40.1	62.2
30CFO/ S550	81.4	86.6	0.094	9.97	71.5	47.3	53.8

3.1.5 TEM micrograph

Images of TEM and EDX analysis for 20CFO/Silica 550, are shown in **Fig. 7** Confirm that microscopic particles have a regular spherical shape with a size range of 200-600 nm. Many particles of CFO are present as single ones; some other particles are aggregating into small aggregates. EDX spectra for 20CFO/Silica550 show the presence of C,Si, Ce,Fe, and O in the silica matrix.

3.1.6. Catalytic measurements

The catalysts' catalytic activity was investigated under optimal reaction conditions. towards the dehydration reaction of isopropyl alcohol (IPA) in the flow of an air atmosphere in a flow bed catalytic reactor. The catalytic activity results at 250 C were investigated and are shown in Fig.8. Results reveal very high catalytic activity for the composite materials, whereas very low catalytic activity was obtained for the blank silica support.

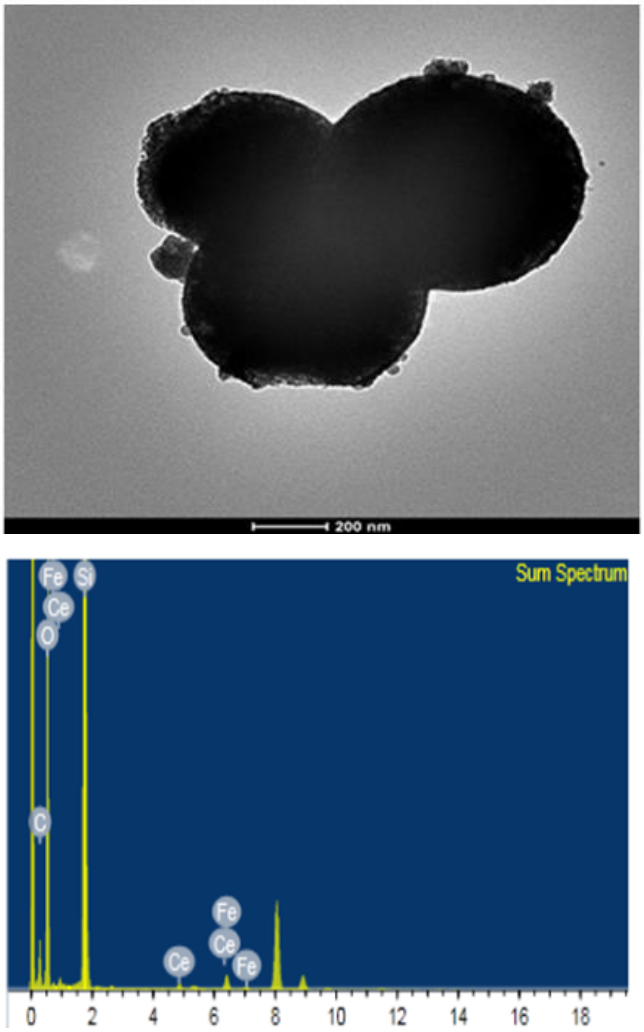

Fig. 7: TEM micrograph and EDX Spectra for 20/CFO silica550.

The catalytic activity was in the order of 20CFO/silica > 30CFO/silica>10CFO/silica>>CFO> silica. The 20CFO/Silica catalyst showed the highest catalytic activity with conversion percent 89.0% at 250 °C and 100% selectivity for propene formation. The superior catalytic material (20CFO/Silica550) was examined in the temperature range of 120–250ºC shown in **Fig. 9**. Increasing the temperature of the catalytic reaction enhances the conversion to propene over the 20CFO/Silica550. It demonstrates that CFO mixed oxide phase loading enhanced surface activity in terms of increasing the acidic sites and enhancement of the surface oxygenated groups. As well known, IPA reaction over the surface of the catalyst only screens the total acidity. To distinguish between the two types of acidic sites and estimate the nature and strength of these sites. Therefore, the chemisorption of basic probe molecules such as pyridine (PY), and dimethyl pyridine (DMPY), was utilized for testing and distinguishing between Lewis (L), and Brønsted (B) acid sites. The effect of admission time of pyridine (PY), and dimethyl pyridine (DMPY) during the dehydration of IPA, at reaction temperature 200 ºC, for 20 CFO/Silica 550, is shown in **Fig. S1**. reveals that the IPA conversion decreases with increasing admission time of PY and DMPY vapors. IPA conversion continuously reduces to reach a steady state of conversion 26% after 35 minutes, respectively. In addition, the conversions in the case of PY and DMPY are overlapped indicating that the nature of these acid sites is mainly due to Brønsted acid sites[48].

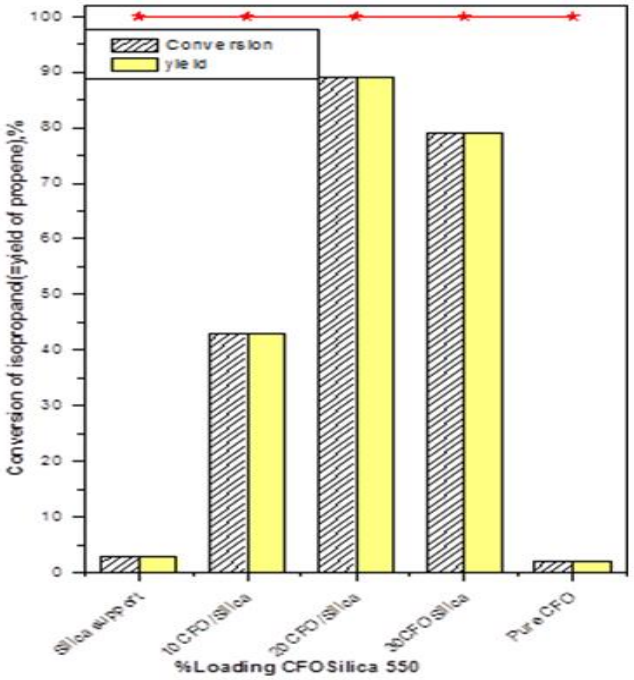

Fig. 8: Catalytic dehydration of isopropanol of IPA for calcined10,20 and 30CFO/Silica along with Silica support and pure CFO 550.

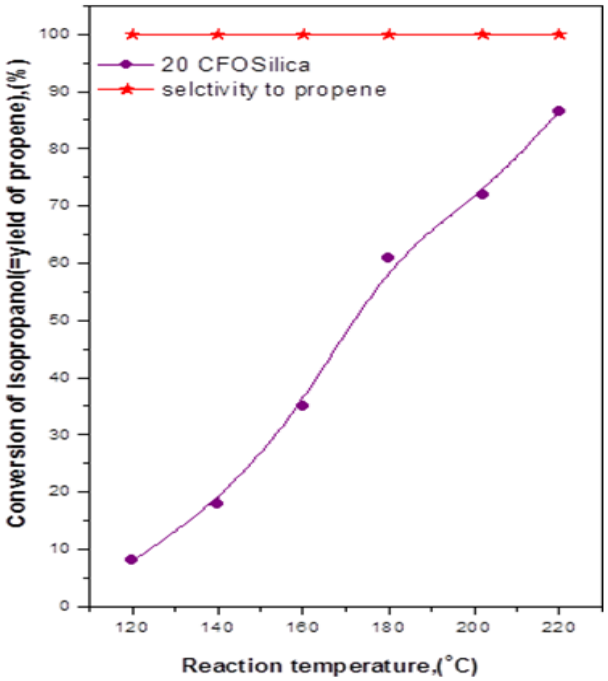

Fig. 9: Catalytic temperature on catalytic performance over 20 CFO/ Silica 550 towards dehydration of isopropyl alcohol into propene.

Table. 2: Comparison between the catalytic performance of the present work and the other literature.

Catalysts	Reaction temperature (C)	IPA Conversion (%)	Propylene selectivity	Ref.
Zr-SBA-15	250	96	100	[49]
Pd/AlGa-x	300	>95	97	[50]
SiO2-ZrO_2	300	90	100	[8]
Fe_3O_4 /γ-Al_2O_3 acid	250	63	45	[14]
Fe_3O_4–CuO/γ-Al_2O_3 basic	290	70	100	[14]
^{t}NP13	260	57	>99	[51]
CFO/Silica 550	250	89	100	Our work

4. Conclusion

The present work showed the investigation of dispersion of different ratios (10 to 30) % of CFO mixed oxides into the silica matrix. The appearance of CFO mixed oxide dispersion nanoparticles or even clusters on the silica support's surface resulted in the formation of a mesoporosity texture of non-porous silica with enhanced surface area and porosity. Amorphous mixed oxide formation or perovskite of CFO into silica matrix enhanced the surface acidity of silica matrix and improved the catalytic dehydration of isopropyl alcohol to propene. The 20 CFO/Silica 550 displayed a high conversion percent and remarkable selectivity in the production of propene. This approach demonstrated that the effective dehydration catalyst towards propene production can be formed by the dispersion of amorphous CFO mixed oxide into silica support. The validated performances of the presented novel 20 CFO/Silica 550 composite catalysts, on the other hand, motivate additional research into surface fine structure which is related to catalytic reaction conditions.

CRediT authorship contribution statement:

Walaa A. Elhamdy: Conceptualization, Methodology, Supervision, Writing – original draft, Investigation, Formal analysis, Data creation, Writing – review & editing. Abd-El-Aziz.A.Said:Supervision,Methodology,Visualization. Kamal M.S. Khalil: Supervision,Visualization, Validation, Investigation.

Data availability statement

The data used to support the findings of this study are available from the corresponding author upon request.

Declaration of competing interest

The authors declare that they have no known competing financial interests or personal relationships that could have appeared to influence the work reported in this paper.

5. References

[1] P. Lu, X. Chang, W. Yu, Q. Hu, K.M. Ali, C. Xing, C. Du, Z. Yang, S. Chen, *Renew. Energy*., 209 (2023) 546–557.

[2] H. Huang, H. Wang, H. Zhu, S. Zhang, Q. Zhang, C. Li, *Catal. Sci. Technol*., 9 (2019) 2203–2210.

[3] L. Xu, R. Zhao, W. Zhang, *Appl. Catal. B Environ.*, 279 (2020) 119389.

[4] A. Ghosh, K. Bhaduri, S. Shah, A. Auroux, J.K. Pandey, *Mol. Catal.*, 475 (2019) 110470.

[5] L.A. Perea, M. Felischak, T. Wolff, J.A. López Gaona, C. Hamel, A. Seidel-Morgenstern, Fuel. 284 (2021) 119031.

[6] G. Goyal, J.N. Kuhn, G.P. Philippidis, *Biomass and Bioenergy*. 108 (2018) 252–257.

[7] Y. Li, Y. Ma, Q. Zhang, V.A. Kondratenko, G. Jiang, H. Sun, S. Han, Y. Wang, G. Cui, M. Zhou, Q. Huan, Z. Zhao, C. Xu, G. Jiang, E. V Kondratenko, *J. Catal.*, 418 (2023) 290–299.

[8] H.-K. Min, Y.W. Kim, C. Kim, I.A.M. Ibrahim, J.W. Han, Y.-W. Suh, K.-D. Jung, M.B. Park, C.-H. Shin, *Chem. Eng. J.*, 428 (2022) 131766.

[9] C. Lacerda, A. Barrios, R. Sousa, T. França, R. Souza, W. Gonzalez, N. Essayem, E. Lachter, *React. Kinet. Mech. Catal.*, 124 (2018) 317–334.

[10] E. Hong, H.-I. Sim, C.-H. Shin, *Chem. Eng. J.*, 292 (2016) 156–162.

[11] J. Escobar, J.A. De Los Reyes, T. Viveros, M. Valle-Orta, M.C. Barrera, *Fuel*, 149 (2015) 109–117.

[12] K.M.S. Khalil, W.A. Elhamdy, M.N. Goda, A.E.A. Said, , *J. Environ. Chem. Eng*., 9 (2021) 106572.

[13] H. Hasanudin, W.R. Asri, L. Andini, F. Riyanti, A. Mara, F. Hadiah, Enhanced Isopropyl Alcohol Conversion over Acidic Nickel Phosphate-Supported Zeolite Catalysts, ACS Omega. 7 (2022) 38923–38932.

[14] M.A. Armenta, R. Valdez, R. Silva-rodrigo, A. Olivas, *Fuel*, 236 (2019) 934–941.

[15] R. Rubab, S. Ali, A. Ur, S. Akram, A. Muhammad, *Colloids Surfaces A Physicochem. Eng. Asp*., 615 (2021) 126253.

[16] A. Finiels, F. Fajula, V. Hulea, *Catal. Sci. Technol.*, 4 (2014) 2412–2426.

[17] D.P. Serrano, J. Aguado, J.M. Escola, *ACS Catal*., 2 (2012) 1924–1941.

[18] C. Krutpijit, P. Tochaeng, B. Jongsomjit, *Catal. Commun.*, 145 (2020) 106102.

[19] P. Decyk, M. Trejda, M. Ziolek, J. Kujawa, K. Głaszczka, M. Bettahar, S. Monteverdi, M. Mercy, *J. Catal.*, 219 (2003) 146–155.

[20] P.A. Torresi, V.K. Díez, P.J. Luggren, J.I. Di Cosimo, Appl. Catal. A Gen. 458 (2013) 119–129. https://doi.org/https://doi.org/10.1016/j.apcata.2013.03.031.

[21] K.M.S. Khalil, W.A. Elhamdy, A.E.-A.A. Said, A.A. Elsamahy, *Colloids Surfaces A Physicochem. Eng. Asp.*, 506 (2016) 840–848.

[22] K.M.S. Khalil, W.A. Elhamdy, A.E.A.A. Said, *Mater. Chem. Phys*,. 254 (2020) 123412.

[23] S. Hosaka, E. Kurniawan, Y. Yamada, S. Sato, A*ppl. Catal. A, Gen*. 653 (2023) 119079.

[24] W.-J. Jeon, H. Kim, S.-H. Byeon, *Colloids Surfaces A Physicochem. Eng. Asp*., 640 (2022) 128416.

[25] Y. Shan, Y. Liu, Y. Li, W. Yang, *Sep. Purif. Technol*., 250 (2020) 117181.

[26] M.R. Nava, C.A.A. Pereira, R. Brackmann, G.G. Lenzi, D.T. Dias, É.C.F. de Souza, J.F.M. Borges, J.B.M. da Cunha, M. Barreto-Rodrigues, *J. Photochem.*

Photobiol. A Chem., 428 (2022) 113839.

[27] Y. Chen, J. Li, W. Teng, H. Wu, W. Liu, S. Ren, J. Yang, Q. Liu, Fuel. 353 (2023) 129179.
[28] H.A. Ahmad, S.S. Ahmed, O. Amiri, Int. J. Hydrogen Energy., 48 (2023) 3878–3892.
[29] Y. Ma, X. Tang, F. Gao, H. Yi, S. Zhao, Y. Shi, C. Wang, *J. Chem. Technol. Biotechnol.*, 95 (2020) 232–245.
[30] C. Chen, X. Yan, B.A. Yoza, T. Zhou, Y. Li, Y. Zhan, Q. Wang, Q.X. Li, Sci. Total Environ. 612 (2018) 1424–1432.
[31] Y. Guan, G. Zhang, R. Wang, Y. Wang, Y. Liu, Fuel. 357 (2024) 129832.
[32] S. Ma, S. Chen, M. Zhu, Z. Zhao, J. Hu, M. Wu, S. Toan, W. Xiang, *Int. J. Hydrogen Energy*., 44 (2019) 6491–6504.
[33] J. Ameta, A. Kumar, R. Ameta, V.K. Sharma, S.C. Ameta, *J. Iran. Chem. Soc*,. 6 (2009) 293–299.
[34] C.E. Choong, C.M. Park, Y.-Y. Chang, J. Yang, J.R. Kim, S.-E. Oh, B.-H. Jeon, E.H. Choi, Y. Yoon, M. Jang, Chem. Eng. J. 427 (2022) 131406.
[35] M.G. Jang, S. Yoon, D. Shin, H.J. Kim, R. Huang, E. Yang, J. Kim, K.-S. Lee, K. An, J.W. Han, A*CS Catal.*, 12 (2022) 4402–4414.
[36] Z. Wang, J. Pang, L. Song, X. Li, Q. Yuan, X. Li, S. Liu, M. Zheng, *Ind. Eng. Chem. Res*., 59 (2020) 22057–22067.
[37] K. Vikrant, K.-H. Kim, *Sci. Total Environ.*, 904 (2023) 166882.
[38] W. Zhu, X. Chen, Z. Liu, C. Liang, *J. Phys. Chem. C.*, 124 (2020) 14646–14657.
[39] Y. Zeng, Y. Wang, S. Zhang, Q. Zhong, *J. Colloid Interface Sci.*, 580 (2020) 49–55.
[40] S. Royer, D. Duprez, F. Can, X. Courtois, C. Batiot-Dupeyrat, S. Laassiri, H. Alamdari, *Chem. Rev.*, 114 (2014) 10292–10368.
[41] W. Stöber, A. Fink, E. Bohn, *J. Colloid Interface Sci.*, 26 (1968) 62–69.
[42] K.M.S. Khalil, A.A. Elsamahy, M.S. Elanany, *J. Colloid Interface Sci.*, 249 (2002) 359–365.
[43] K.M.S. Khalil, L.A. Elkabee, B. Murphy, *J. Colloid Interface Sci.*, 287 (2005) 534–541.
[44] S. Brunauer, P.H. Emmett, E. Teller, *J. Am. Chem. Soc.*, 60 (1938) 309–319.
[45] E.P. Barrett, L.G. Joyner, P.P. Halenda, *J. Am. Chem. Soc*., 73 (1951) 373–380.
[46] R.A. Sing, K.S.W., Everet, D. H., Haul, *Pure Appl. Chem.*, 57 (1985) 603–619.
[47] A.E.A. Said, K.M.S. Khalil, *J. Chem. Technol. Biotechnol.*, 75 (2000) 196–204.
[48] S. Pyen, E. Hong, M. Shin, Y. Suh, C. Shin, *Mol. Catal.*, 448 (2018) 71–77.
[49] M. Murat, Zdenˇ, E. Tišler, J. Šimek, J.M. Hidalgo-Herrado, Catalysts. (2020) 719.
[50] J.N. Díaz de Leon, A. Cruz-Taboada, Y. Esqueda-Barron, G. Alonso-Nuñez, S. Loera-Serna, A.M. Venezia, M.E. Poisot, S. Fuentes-Moyado, *Catal. Today.*, 356 (2020) 339–348.
[51] A. Ghosh, K. Bhaduri, S. Shah, A. Auroux, J.K. Pandey, B. Chowdhury, *Mol. Catal.*, 475 (2019) 110470.